Estimation of Single-Neuron Model Parameters from Spike Train Data

Randall D. Hayes[1,3], John H. Byrne[1], Steven J. Cox[2] and Douglas A. Baxter[1,4]

[1]Center for Computational Biomedicine

Department of Neurobiology and Anatomy

The University of Texas-Houston Medical School

6431 Fannin Street, Houston, TX 77031

[2]Computational and Applied Mathematics

Rice University

6100 Main Street, Houston, TX 77005

[3]W.M. Keck Center for Computational and Structural Biology, Houston, TX 77005

[4]Corresponding author

E-mail: Douglas.Baxter@uth.tmc.edu

ABSTRACT

Estimating parameters for models of neurons requires a quantitative comparison between the model output and empirical data. The present study compares three error functions: voltage-time-series (VTS), cumulative-voltage-integrals (CVI), and phase-histograms (PH). In two test cases, predefined models were used to produce target data and to compare the efficacy of the three error functions when they were used to recover the target data. In a third example, empirical data were used to parametrize a model. VTS was found to be inferior, whereas as CVI and PH were similar and effective. Reliable parameters were derived from analyzing as few as two datasets.

KEYWORDS

parameter estimation; action potentials; central pattern generator; *Aplysia*; electrophysiology

INTRODUCTION

Models of neurons and neural circuits are important tools for synthesizing large amounts of disparate empirical data within a dynamical framework that allows for quantitative evaluation of hypotheses of neural function. Moreover, models can provide predictions that guide empirical studies. The value of a model, however, is related to its ability to accurately recapitulate biological function. Although in a few

instances neurons or neural circuits have been characterized in sufficient detail to adequately parameterize a model [1,2,4,5,13,14,16,22], more often building models requires estimation of parameters from limited, less than ideal data sets. It would be particularly useful if it was possible to adequately parametrize models using commonly available current-clamp data, such as recordings of spike trains. However, spike trains have properties that are difficult to fit with existing methods. For example, empirical recordings of spike trains often have irregular interspike intervals, and these relatively minor irregularities can make a disproportionate contribution to the error function, which in turn can cause parameter search algorithms to recover less than optimal values for parameters. Such current-clamp data require error functions that are robust to variations in interspike intervals. The present study compares three methods for generating error functions and examines which method is best suited for analyzing spike train recordings.

Error Functions

An error function compares the output of a model to a target dataset. One of the main problems for optimization algorithms is the presence of local minima in the error function, which can force the algorithm to terminate on less than optimal parameter values. Stochastic optimization algorithms get around this problem by occasionally randomly changing parameter values, allowing the algorithm to escape local minima [3,7,10]. One of our goals in trying different error functions was to eliminate the occurrences of local minima, because the optimization program used here is not stochastic [6]. Fig. 1 illustrates the three error functions that were used in the present study.

Voltage time-series (VTS). The VTS error function simply subtracts one trace from another at each time point and squares the differences so that they will always be positive (Fig. 1A).

$$E_{VST} = \int_0^T \left\| v_{\text{model}} - v_{\text{data}} \right\|^2 dt$$

(1)

The underlying reason is that any measure of mismatch can be conceived of as a distance from the model point to the target point in some multidimensional parameter space, and distances must be positive [17]. VTS works well for fitting smoothly varying processes such as hyperpolarizing current injections, single post-synaptic potentials or single action potentials recorded at high time resolution. However, when fitting narrow peaks, such as trains of action potentials, the voltage time-series is vulnerable to phase-shift errors [17]. Even an identical waveform, slightly shifted in time, will produce a large squared error. Note the double peaks in squared error in Fig. 1A4. An optimization scheme using this function, in trying to reduce

the error, is prone to settling into local minima in silent (non-spiking) regions of parameter space, removing one of the double peaks in the error function but leaving the other and producing a poor overall fit to the data. The same problem could result from a situation where the model was time-locked to the first spike in the data but was firing at a different frequency than the cell that produced the data.

Cumulative Voltage Integral (CVI). One way to deal with the phase-shift problem is to smooth the data somewhat by summing the individual traces over time. This procedure has the effect of broadening the peaks in the error function (Fig. 1C).

$$E_{CVI} = \int_0^T \left\| \int_0^t v_{model} - \int_0^t v_{data} \right\|^2 dt \tag{2}$$

Phase Histogram (PH). A different way to deal with the phase-shift problem is to ignore the time dimension entirely, instead plotting the membrane voltage vs. its time-derivative in the phase plane [17]. Summing the plotted points at each combination of voltage magnitude and voltage slope produces a phase histogram (also called a trajectory density function) (Fig. 1B). Subtracting the two phase histograms and squaring the differences produces an error function that is sensitive to spike shape and spike frequency and that is robust to differences in spike phase.

$$E_{PH} = \int_{-80}^{50} \int_{-10^4}^{10^4} \left\| flag\left(v, \frac{dv}{dt}\right)_{model} - flag\left(v, \frac{dv}{dt}\right)_{data} \right\|^2 dv, d^2v \tag{3}$$

The PH error function has been used previously in neural models, in optimization of single parameters such as maximum conductances and half-activation voltages [17]. Here we extend its use to searching for multiple parameters at the same time (up to 11 parameters at a time).

METHODS

Software

The present study used two software packages: the neurosimulator SNNAP and the parameter estimation program PEST. The neurosimulator was used to produce target data during the evaluation of the three error functions. In addition, a small Java program generated the PH functions from SNNAP's ASCII output files.

SNNAP (Simulator for Neural Networks and Action Potentials). SNNAP was designed as a tool for the rapid development and simulation of realistic models of single neurons and neural networks [12,25]. The electrical properties of individual neurons are described with Hodgkin-Huxley type voltage- and time- dependent ionic currents. For this paper SNNAP was modified slightly so that the program terminated automatically upon finishing a simulation. This modification was necessary to allow the program to be run iteratively by the optimization program described below. As of this writing, the modified version of SNNAP can be obtained from the authors. SNNAP is freely available at http://SNNAP.uth.tmc.edu.

PEST (Parameter ESTimation). PEST is a Windows-executable program that acts as a shell around a simulator, such as SNNAP. The simulator is called through a line command that in this case consists of three elements: the invocation of java, the name of a java archive (*.jar) file such as SNNAP, and the pathname of the simulation input files. PEST interacts with the simulator through ASCII input and output files, a feature that makes it particularly convenient to use with SNNAP. PEST uses a Gauss-Levenberg-Marquardt method of parameter estimation [6]. For nonlinear problems, such as the Hodgkin-Huxley equations, parameter estimation is iterative. During each iteration, the relationship between model parameters and model output is linearised by formulating it as a Taylor expansion about the currently best parameter set. PEST then increments each parameter and runs the model n times in order to fill a $m \times n$ Jacobean matrix of partial derivatives, where m is the number of state variables and n is the number of parameters. This linearized problem is then solved for a better parameter set, and the new parameters are tested by running the model again. PEST is freely available at http://www.sspa.com.

Models

Three models were examined. The first was the conventional Hodgkin and Huxley [14] mode of a placed clamped squid axon. The second was an unpublished model that was developed to replicate the firing properties of identified neuron B34 in the buccal ganglia of *Aplysia* [15]. The third was model developed in the present study to test the ability of the SNNAP/PEST interactions to fit empirical data and parameterize a model. The empirical data were unpublished intracellular recordings of spike trains from identified cell CBI-2 in the cerebral ganglia of *Aplysia* [19,21].

Hodgkin-Huxley model (HH model). The HH model included a fast Na^+ (g_{Na}) and delayed K^+ (g_K) conductances, which underlie spiking [14]. Activation and inactivation variables (m^3 and h, respectively, for g_{Na} and n^4 for g_K) were calculated from rate-constant expressions (i.e., α and β). The target dataset were

the standard parameters for an action potential at 6.8°C and one cm^2 of membrane (see Table 1). The HH model input files that were used for simulations in the present study are available at the SNNAP web site.

Aplysia **cell B34.** There were two fundamental differences between the HH model and the B34. First, in addition to including fast Na$^+$ (g_{Na}) and delayed K$^+$ (g_K) conductances, the B34 model also included a transient, A-type K$^+$ conductance ($g_{K,A}$). Second, that activation and inactivation variables for these conductances were modeled with time-constant expressions after the methods of Byrne [4,5], which utilize Boltzman functions rather that rate-constant functions. The target parameters are detailed in Table 1.

Aplysia **cell CBI-2.** To test the optimization procedures on empirical data, we created a third model cell, whose parameters are also listed in Table 1. This cell was constructed in two steps. First, capacitance and g_L, the maximum leak conductance, were set by matching the response of model to hyperpolarizing currents (-1 to –5 nA) to those recorded from a CBI-2 neuron in a reduced preparation of the isolated cerebral ganglia (data supplied by R. Mozzachiodi). In a second step, maximum conductance and activation/inactivation parameters for the voltage-dependent conductances, which included g_{Na} and g_K, were fit by PEST.

Error Functions

VTS and **CVI**. These functions sampled SNNAP simulations every 10 time-steps (i.e., data were sampled every 200 μs) and thus consisted of 13,170 points.

PH. Membrane voltage (-80 to +50mV, 13,170 points) was quantized into 10 mV bins. The time-derivative of membrane voltage (dV/dt) was quantized into bins of 10^2 mV/s (-10^3 to +10^3, 13,170 points). This resulted in a 14 × 21 grid in the phase plane, which was concatenated into a 1 × 294 vector for use with PEST.

RESULTS

Error Functions

Fig. 2 illustrates the various error functions for current injection into the B34 model. For these simulations, a single parameter, either the maximum conductance to Na$^+$ or K$^+$, was varied systematically (g_{Na} in Panel **A** and g_{KA} in Panel **B**). In both cases, the VTS showed a narrow well around the true conductance value, meaning that only close matches to the true value reduced the value of the error function substantially. The gradient of the error function was nearly flat along one side of the VTS function,

rendering optimization difficult. In addition, the VTS showed local minima, which can force a non-stochastic optimization program such as PEST to terminate on non-optimal parameter values. Interestingly, both local minima were seen in regions of silence, where the model was not firing action potentials. This finding is a biologically relevant extension of LeMasson and Maex [17], who demonstrated local minima only with pure phase-shifts between identical spike trains. Minima occurred at lower values of g_{Na} and higher values of g_{KA}, since both of these manipulations reduce the model's excitability.

In contrast, both the PH and the CVI functions showed a single minimum at the true value of the maximum conductance, 14 μS. Both functions varied smoothly and gradually, which would be expected to improve optimization efficiency. Of course, the behavior of the functions in these single dimensions is no guarantee that they will not have local minima in nonlinear, multidimensional parameter spaces such as those possessed by neural cell models.

Estimation of conductance parameters

Having confirmed that the PH function was superior to the VTS and equal to the CVI, we used the PH for the rest of these experiments. Previous studies earlier demonstrated the utility of the PH in recovering single model parameters [17]. Here we extend its use, first to three parameters, then to 11 parameters. Table 1 indicates the performance of the PH in recovering the values of three maximum conductance parameters (g_{Na}, g_K, and $g_{K,A}$) from a simulated B34 spike train.

Estimation of half-activation voltages

We next subjected the PH to a more stringent test, asking it to simultaneously recover the values of 3 maximum conductances and 8 activation/inactivation parameters from the two spike train datasets from B34. The responses to 3 and 8 nA of injected current were used for the analysis (see Fig. 3B). This is a more difficult condition for the optimization algorithm because when more parameters are fitted, multiple parameter combinations may be able to satisfy the data. The initial values of the parameters, the estimated parameters, and the target data that generated the spike train data are listed in Table 1.

Finally, we used the PH to estimate the same 11 parameters from experimental data for cell CBI-2. The values of the initial and estimated parameters are listed in Table 1 (see Fig. 3C).

Input-Output Curves

We tested the robustness of the optimized parameters by injecting a series of constant currents (1-10 nA) into the HH and B34 models. The results of this experiment are illustrated in Fig. 3. For the HH and

B34 models, the recovered current-frequency curves were quite similar to the target data, even at currents that were not used in the PEST fit. However, as illustrated in Table 1, the recovered parameter values for the HH and B34 models were similar to but not identical to the target parameters. Indeed, some cases the target data and recovered parameters differed as much as 50%. This result suggests that there may be no unique solution to the current-frequency relationship for these cells, a finding supported by previous modeling work in other systems (see Discussion). In addition to re-parametrizing predefined models, PH and parameter estimation algorithm were able to parametrize the CBI-2 model in such a way as to accurately recapitulate the empirical data over a wide range of spiking behaviors (Fig. 3C).

DISCUSSION

In previous studies, several error functions have been used for parameter searches of voltage-dependent conductances, including simple subtraction of the two voltage traces [23,24], lists of spike times extracted from voltage traces [8,24], and Fourier-transformed voltage traces in the frequency domain [23]. Any function that matches time-based waveforms should be somewhat sensitive to the local minima described above (although the performance of the cumulative voltage integral was very robust). Most of these previous studies used stochastic optimization algorithms, which are less sensitive to local minima, but which require many thousands of model runs in order to correctly estimate model parameters. Use of error functions without local minima allowed PEST to estimate a modest number of model parameters. For the cases used for the present study, solutions were achieved with usually <30 PEST iterations, which invoked <1000 SNNAP simulations. Also in development are substantially faster techniques for solving the gradient of the error function directly, rather than repeatedly approximating the partial derivative of each parameter as PEST does [11].

PEST was successful in estimating parameter subsets in model-generated data with as little as two datasets. We were unable to uniquely determine all of the parameters of CBI-2 from a single dataset, which is not necessarily surprising. Many complex systems do not have unique solutions, often because increases in one parameter can be offset by decreases in another. It has been shown in the case of conductance-based neuron models that multiple combinations of parameters can lead to similar output [8,9]. When working with limited data, it may not be possible uniquely determine every parameter. However, for functional studies of neural circuits, it may not be necessary to do so. Matching the input-output characteristics of neurons may be adequate for some purposes, such as simulated lesion

experiments when one neuron is simply removed from a circuit to determine its contribution to a motor output [18].

The most commonly used methods for parametrizing models are still trial-and-error and fit-by-eye, a strategy that can be quite successful for relatively simple models. As models and datasets continue to grow in size and complexity, however, automated parameter search methods will become common through sheer necessity (however see [20] for an alternative database approach). This transition will be eased by simple, robust methods that work with traditional experimental data such as those derived from current injection.

ACKNOWLEDGEMENTS

Randall Hayes majored in biology at the University of Kentucky. He studied neuroscience at the University of Rochester. In 2001, he received a Ph.D. for his work on "*Ideal Observer Analyses of Cortical Lesions in Macaques and Humans.*" He is currently a Keck Fellow, and is using computer simulations to study learning in invertebrate neural networks.

John H. Byrne received the Ph.D. degree in bioengineering from the Polytechnic Institute of Brooklyn in 1973. He conducted his postdoctoral training at the College of Physicians and Surgeons at

Columbia University under the guidance of Nobel Laureate E. Kandel. Dr. Byrne is currently the Professor, June and Virgil Wagner Distinguished Chair, and Chairman of the Department of Neurobiology and Anatomy, and he is the Director of the Neuroscience Research Center at The University of Texas-Houston Medical School. His research focuses on elucidating the cellular and molecular processes that underlie learning and memory.

       Steven J. Cox received the Ph.D. degree in Mathematics from Rensselaer Polytechnic Institute in 1988. He conducted postdoctoral work with Michael Overton at the Courant Institute for Mathematical Sciences at NYU.

       Douglas A. Baxter received the Ph.D. degree in zoology from The University of Texas at Austin in 1981. He conducted postdoctoral training in the laboratories of D. Johnston at Baylor College of Medicine and J. H. Brown at the Beckman Research Institute City of Hope. Currently, Dr. Baxter is an Associate Professor of Research in the Department of Neurobiology and Anatomy, The University of Texas-Houston Medical School. His research uses a combination of computational and experimental approaches to investigate the neural basis of behavior and behavioral modifications.

REFERENCES

[1]   M. Bazhenov, M. Stopfer, M. Rabinovich, R. Huerta, H.D. Abarbanel, T.J. Sejnowski, G. Laurent (2001a). Model of transient oscillatory synchronization in the locust antennal lobe. Neuron, 30: 553-567.

[2]   M. Bazhenov, M. Stopfer, M. Rabinovich, H.D. Abarbanel, T.J. Sejnowski (2001b). Model of cellular and network mechanisms for odor-evoked temporal patterning in the locust antennal lobe. Neuron, 30: 569-581.

[3]   V.A. Booth (1999). A generic algorithm study on the influence of dendritic plateau potentials on bistable spiking in motoneurons. Neurocomput. 26: 69-78.

[4]   J.H. Byrne (1980a). Analysis of ionic conductance mechanisms in motor cells mediating inking behavior in *Aplysia californica*. J. Neurophysiol. 43: 630-650.

[5]   J.H. Byrne (1980b). Quantitative aspects of ionic conductance mechanisms contributing to firing pattern of motor cells mediating inking behavior in *Aplysia californica*. J. Neurophysiol., 43: 651-668.

[6]   J. Doherty (2002). PEST User's Manual. Brisbane, Australia, Watermark Numerical Computing.

[7]   R.M. Eichler-West, E. DeSchutter, G.L. Wilcox, Using evolutionary algorithms to search for control parameters in a nonlinear partial differential equation. In: L.D. Davis, K. DeJong, M.D. Vose, L.D. Whitley, eds., Evolutionary Algorithms, Vol. 111 of the IMA Volumes in Mathematics and its Applications (Springer-Verlag, New York, 1999) 33-64.

[8]   W.R. Foster, L.H. Ungar, J.S. Schwaber (1993). Significance of conductances in Hodgkin-Huxley models. J. Neurophysiol. 70: 2502-2518.

[9]   M.S. Goldman, J. Golowasch, E. Marder, L.F. Abbott (2001). Global structure, robustness, and modulation of neuronal models. J. Neurosci. 21: 5229-5238.

[10]   D. Goldberg, Algorithms in Search, Optimization and Machine Learning (Addison-Wesley, New York, 1989).

[11]   A. Griewank, A. Walther (2001). On constrained optimization by adjoint based quasi-Newton methods. Optim. Methods Softw. 17: 869-889.

[12]   R. Hayes, J.H. Byrne, D.A. Baxter, Neurosimulation: Tools and resources. In: Arbib, M.A. ed., The Handbook of Brain Theory and Neural Networks, Second Edition (Cambridge, MIT Press, 2003) 776-780.

[13]   A.A Hill, J. Lu, M.A. Masino, O.H. Olsen, R.L. Calabrese (2001). A model of a segmental oscillator in the leech heartbeat neuronal network. J. Comput. Neurosci., 10: 281-302.

[14]   A.L. Hodgkin, A.F. Huxley (1952). A quantitative description of membrane current and its application to conduction and excitation in nerve. 117: 500-44.

[15]   I. Hurwitz, I. Kupfermann, A.J. Susswein (1997). Different roles of neurons B63 and B34 that are active during the protraction phase of buccal motor programs in *Aplysia californica*. J. Neurophysiol. 78: 1305-19.

[16]   S.H. Jezzini, A.A. Hill, P. Kuzyk, R.L. Calabarese (2003). A detailed model of intersegmental coordination in the timing network of the leech heartbeat central pattern generator. J. Neurophysiol., in press.

[17]   G. LeMasson, R. Maex, Introduction to equation solving and parameter fitting. In: E. DeSchutter, ed., Computational Neuroscience: Realistic Modeling for Experimentalists (New York, CRC Press, 2001) 1-23.

[18]   J.R Lieb, Jr., W.N. Frost (1997). Realistic simulation of the *Aplysia* siphon-withdrawal reflex circuit: roles of circuit elements in producing motor output. J. Neurophysiol. 77: 1249-1268.

[19]   R. Mozzachiodi, H. Lechner, D.A Baxter, J.H. Byrne (2003). An in vitro analogue of classical conditioning of feeding in *Aplysia*. Learn. Mem. 10: 478-494.

[20]   A.A. Prinz, C. Billimoria, E. Marder (2003). An alternative to hand-tuning conductance-based models: construction and analysis of databases of model neurons. J. Neurophysiol. 90: 3998-4015.

[21]   S.C. Rosen, T. Teyke, M.W. Miller, K.R. Weiss, I. Kupfermann (1991). Identification and characterization of cerebral-to-buccal interneurons implicated in the control of motor programs associated with feeding in *Aplysia*. J. Neurosci. 11: 3630-3655.

[22]   M. Steffen, C. Seay, B. Amini, Y. Cai, A. Feigenspan, D.A. Baxter, D.W. Marshak (2003). Spontaneous activity of dopaminergic retinal neurons. Biophy. J., 85: 2158-2169.

[23]   J. Tabak, C.R. Murphey, L.E. Moore (2000). Parameter estimation methods for single neuron models. J. Comput. Neurosci. 9: 215-236.

[24]   M.C. Vanier, J.M. Bower (1999). A comparative survey of automated parameter-search methods for compartmental neural models. J. Comput. Neurosci. 7: 149-171.

[25]   I. Ziv, D.A. Baxter, J.H. Byrne (1994).   Simulator for neural networks and action potentials: description and application. J. Neurophysiol. 71: 294-308.

FIGURE LEGENDS

Fig. 1. Three error functions generated by a 10% change in A-type K$^+$ conductance ($g_{K,A}$). Spike activity was elicited in the model of cell B34 before (**A1**) and after (**A2**) a 10% increase in the value of $g_{K,A}$. **A)** Voltage time-series. A point-by-point subtraction of the voltage traces in Panels **A1** and **A2** produce the error function in Panel **A3**. This error function is squared to produce the function in Panel **A4**, which provides the numerical input to the optimization program. **B)** Phase histogram. The data in Panels **A1** and **A2** were projected into the V:*dV/dt* phase plane and phase histograms were generated (Panels **B1** and **B2**, respectively). An error function (Panel **B3**) was generated using Eq. 3. **C)** Taking the cumulative integral of the two voltage traces before subtraction broadens and smoothes the resulting error function, which provided numerical input to the optimization program.

Fig. 2. Systematic manipulation of single maximum conductance variables in the B34 model. Summed squared error for each function, normalized by each function's maximum, is plotted vs. maximum conductance. **A)** Sodium conductance. **B)** A-type potassium conductance. In both cases, the VTS shows local minima in regions of silence, where the cell does not spike. Both the CVI and the PH vary smoothly towards a single minimum.

Fig. 3. Predicted current-frequency curves. **A)** HH model. Parameters extracted from either a single experimental dataset (5 nA or 6 nA) failed to predict the firing rate of HH model across the entire range of injected currents. However, simultaneously fitting parameters to both the 5 nA and 6 nA datasets constrained the model that correctly reproduced the firing rates. **B)** B34 model. Parameters estimated from a single simulated dataset (2 nA injected current) correctly predicted the firing rate of the B34 model to several, but not all, of the injected currents. Similarly, parameters estimated from only the 8 nA dataset correctly predicted the firing rate over limited range of injected currents. However, simultaneously fitting the 2 and 8 nA data sets substantially improved the behavior of model. **C)** Cell CBI-2. A pair of experimental datasets (2 nA and 4 nA) was sufficient to constrain the model parameters in such a way that the model could reproduce experimental firing rates over the range tested.
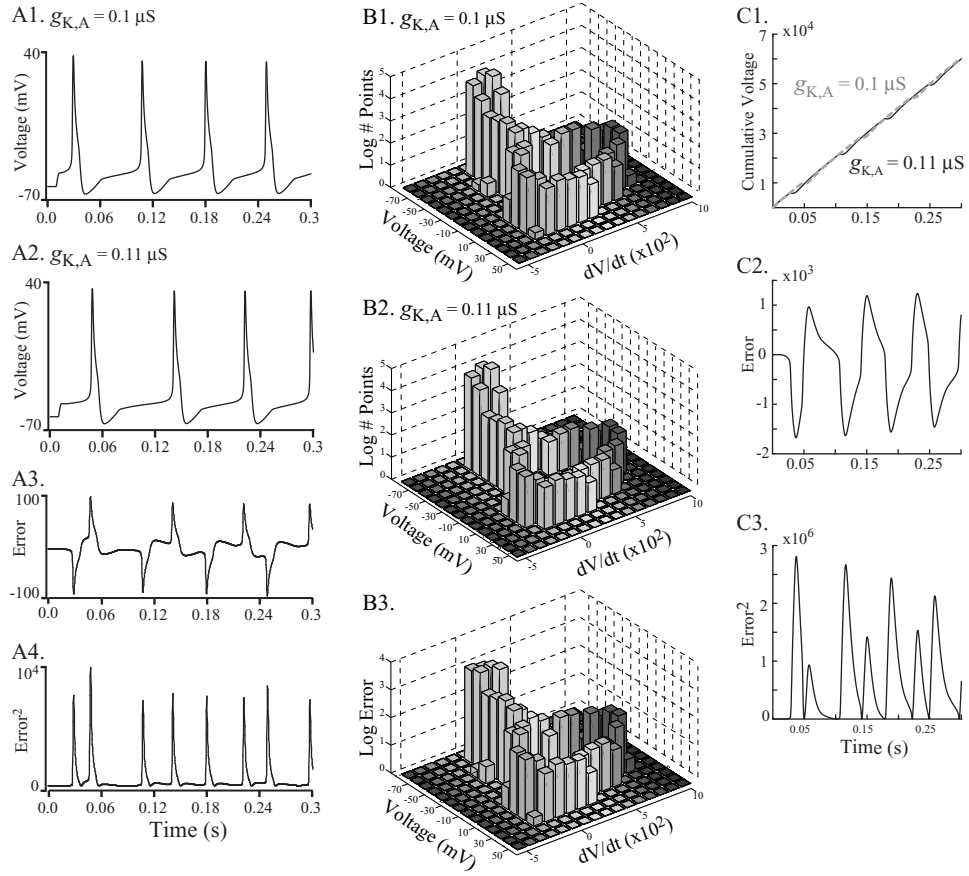
Table 1

B34 Model				
	Initial Value	Final Value	Target Data	Relative Sensitivity
$\overline{g}_{Na}$ (µS)	10.5	7.13	7.5	56.23
$\overline{g}_{K}$ (µS)	35	27.2	25	4.07
$\overline{g}_{K,A}$ (µS)	0.07	0.138	0.1	38.00

HH Model				
	Initial Value	Final Value	Target Data	Relative Sensitivity
g_{Na}				
$\overline{g}_{Na}$ (mScm^{-2})	108	104.37	120	147.97
$V_{1/2}$ of α_m (mV)	38.51	39.18	35.01	189.45
$V_{1/2}$ of β_m (mV)	-54	-56.76	-60	190.40
$V_{1/2}$ of α_h (mV)	-54	-57.58	-60	121.91
$V_{1/2}$ of β_h (mV)	-27	-27.69	-30	121.42
g_{K}				
$\overline{g}_{K}$ (mScm^{-2})	40	43.85	36	172.63
$V_{1/2}$ of α_n (mV)	55.01	49.62	50.01	74.34
$V_{1/2}$ of β_n (mV)	-66	-62.68	-60	169.38

B34 Model					CBI-2 Model		
	Initial Value	Final Value	Target Data	Relative Sensitivity	Initial Value	Final Value	Relative Sensitivity
g_{Na}							
$\overline{g}_{Na}$ (µS)	5.5	12.62	7.5	9.58	14.5	15.76	4.29
$V_{1/2}$ of A_∞ (mV)	-35.1	-38.46	-39	305.45	-43.1	-42.84	113.70

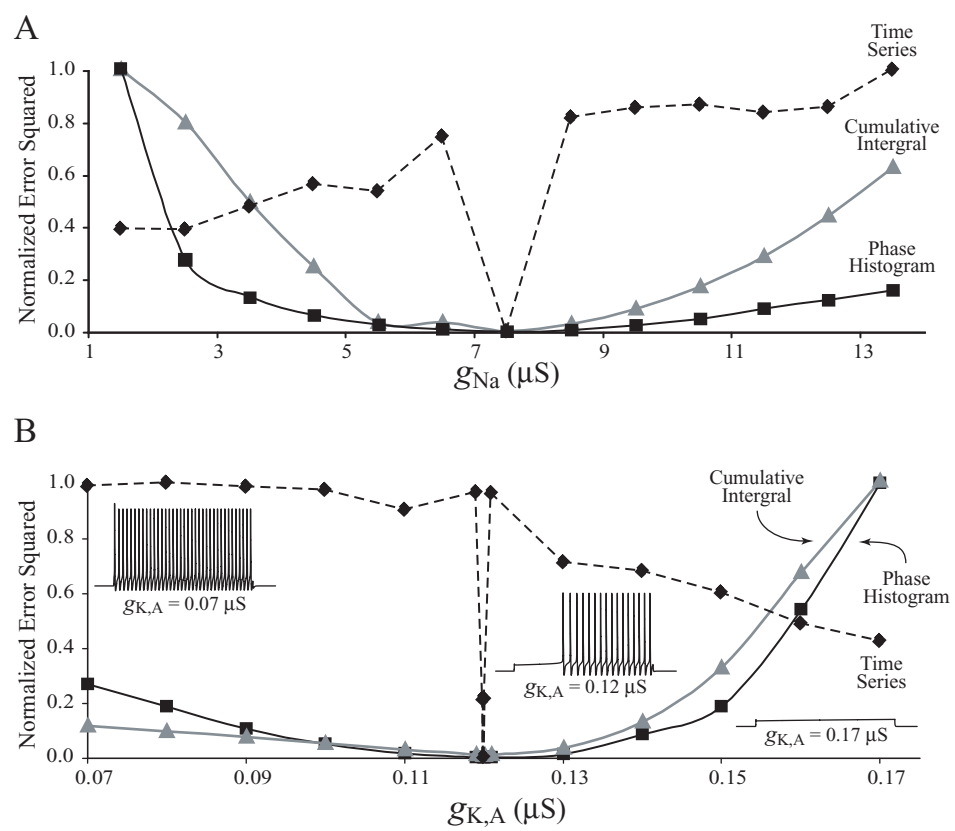|							
V½ of τ_A (mV)	-36	-37.46	-40	133.97	-42	-38.67	3.80
V½ of B_∞ (mV)	-54	-54.16	-36	190.42	-67	-66.12	30.25
V½ of τ_B (mV)	-32	-36.67	-36	2.44	-67.5	-69.62	0.78
g_K							
$\overline{g}_K$ (μS)	20	22.14	25	6.10	25	27.71	1.33
V½ of A_∞ (mV)	-21.3	-21.93	-23	234.66	-31.3	-28.75	2.69
V½ of τ_A (mV)	-8	-15.11	-10	1.39	-23	-21.68	1.57
V½ of B_∞ (mV)	-17.2	-22.52	-14.4	1.75	-26.2	-25.08	0.43
V½ of τ_B (mV)	-17	-15.86	-21	1.34	-33	-26.24	0.69
g_l							
$\overline{g}_l$ (μS)	0.88	0.1	0.1	7.66			

The PH error function was used to recover parameter values from the B34 and HH models and to parameterize a model of CBI-2. Fig. 2 illustrates recovery of a single parameter. The top Panel of Table 1 illustrates simultaneous recovery of three parameters. The lower Panels illustrate the simultaneous recovery of 8 parameters in the HH model and 11 parameters in the B34 model. Target dataset for the HH and B34 models are listed in the column labeled 'Target Data'. In addition, parameters for a model of CBI-2 were predicted from empirical data that was recorded from CBI-2. Since values for CBI-2 were estimated from experimental data, there are no target values. Initial values were perturbed from the target values by +/-20%. Final values are those estimated after 20-40 PEST iterations. PEST also analyzes the relative sensitivity of each parameter [6], and these values are reported for the final PEST iteration.

A. HH Model

B. B34 Model

C. CBI-2 Model